Journal of Statistical Physics, Vol. 80, Nos. 1/2, 1995

Extreme Value Distributions in Chaotic Dynamics

V. Balakrishnan,[1,2] C. Nicolis,[3] and G. Nicolis[1]

Received September 7, 1994; final December 30, 1994

A theory of extremes is developed for chaotic dynamical systems and illustrated on representative models of fully developed chaos and intermittent chaos. The cumulative distribution and its associated density for the largest value occurring in a data set, for monotonically increasing (or decreasing) sequences, and for local maxima are evaluated both analytically and numerically. Substantial differences from the classical statistical theory of extremes are found, arising from the deterministic origin of the underlying dynamics.

KEY WORDS: Extreme value theory; local maxima statistics; fully developed chaos; intermittent chaos.

1. INTRODUCTION

Extreme events are of great importance in a variety of problems in not only the physical, but also the engineering and environmental sciences, from the breakdown of a mechanical structure to the onset of a severe thunderstorm, flooding, or an earthquake.[1,2] Information on their probability distributions is thus of great value in, among others, the design of buildings or bridges or the risk assessment of failure of a machine.

There exists a powerful statistical theory of extremes. In its classical version[3,4] it is concerned with sequences $X_0,..., X_{n-1}$ of independent and identically distributed random variables (iidrv's), and the question asked is the distribution of the largest value found in the sequence, $M_n = \max(X_0,..., X_{n-1})$. Let

$$F(x) = \text{Prob}(X \leqslant x), \qquad a \leqslant X \leqslant b \tag{1.1}$$

[1] Center for Nonlinear Phenomena and Complex Systems, Université Libre de Bruxelles, C.P. 231, 1050 Brussels, Belgium.
[2] Department of Physics, Indian Institute of Technology, Madras 600 036, India.
[3] Institut Royal Météorologique de Belgique, 1180 Bruxelles, Belgium.

822/80/1-2-20

be the cumulative probability distribution of X, with $F(a)=0$, $F(b)=1$ [if a corresponding probability density $\rho(x)$ exists, then $F(x)=\int_a^x \rho(y)\,dy$]. The distribution of M_n is then evidently given by

$$F_n(x)=\text{Prob}(X_0\leqslant x,\ldots, X_{n-1}\leqslant x)=(F(x))^n \tag{1.2}$$

As n increases, the distribution $F_n(x)$ shifts toward increasing values of x, but if appropriately scaled variables are introduced, a limiting form can be attained as $n\to\infty$. A most remarkable result is that under *linear* renormalizations of the form $\{X_i\}\to\{a_n(X_i-b_n)\}$, $a_n>0$, such limiting distributions fall into just three universality classes or types. All of these derive from the generic expression

$$\begin{aligned} H_\beta(x) &= \lim_{n\to\infty} \text{Prob}(a_n(M_n-b_n)\leqslant x) \\ &= \lim_{n\to\infty} [F(a_n^{-1}x+b_n)]^n \\ &= \exp[-(1-\beta x)^{\beta^{-1}}] \end{aligned} \tag{1.3}$$

where $-\infty<\beta<\infty$, $\beta x<1$, and $H_0(x)=\exp(-e^{-x})$. Simple sufficient conditions are known for the existence of such limiting distributions when $F(x)$ has a density function $\rho(x)$.

Intuitively, it would seem that events that are sufficiently rare—as is the case for extreme events—can indeed be reasonably treated as independent of each other. Actually a more elaborate study[5,6] shows that Eq. (1.3) still applies to correlated sequences, essentially as long as the time autocorrelation function falls to zero faster than $1/\ln n$.

It is by now well established that large classes of deterministic dynamical systems governed by nonlinear evolution laws and operating under constraint can give rise spontaneously to complex behavior in the form of abrupt transitions, a multiplicity of states, or (spatio-) temporal chaos.[7] It has been suggested that these phenomena may be at the basis of the variability of the weather and climate,[8,9] which constitute in a sense a universal source of most of the extreme events encountered in our familiar, everyday experience. It is therefore natural to inquire whether a theory of extremes can be built for such systems and, if so, to what extent it either reduces for practical purposes to the classical statistical theory or, in contrast, bears the signature of the deterministic character of the underlying dynamics. Our principal goal in the present paper is to formulate such a theory and to provide a first series of illustrations on simple case studies. As a byproduct, our approach will allow us to handle problems involving

a small or moderate number n of data sets, for which the limiting distributions given by Eq. (1.3) do not apply.

The general formulation is laid down in Section 2, where expressions for the cumulative probability $F_n(x)$ and the associated density $\rho_n(x)$ for the extreme value of sequences generated by an arbitrary one-dimensional recurrence are derived. We show that these functions are piecewise analytic but are nondifferentiable or discontinuous on a set of points that becomes dense as $n \to \infty$. This suggests that there should be substantial differences from the statistical formulation, Eqs. (1.2) and (1.3); a more detailed study, carried out in Sections 3 and 4, corroborates fully this idea.

In Section 3 the general formulation is applied to fully developed chaos. Analytic expressions for F_n for the first few values of n are derived for the logistic, tent, and Bernoulli maps and confronted successfully with the results of numerical simulations. These results bring out clearly the striking differences that exist between extreme value distributions in deterministic chaos and the corresponding classical or "statistical" distributions for iidrv's, even though the time series we consider in the former category are actually δ-correlated. As n is increased, the probability mass shifts toward the right boundary and is eventually concentrated in a layer of width of $O(n^{-1})$. In view of the intricate, increasingly nondifferentiable structure of $F_n(x)$ [or discontinuous structure of $\rho_n(x)$] as n becomes larger and larger, no explicit analytic expression is available in this limit. However, a systematic counting procedure can be worked out which allows one to find both the overall ordered structure of the probability distribution as well as a tractable model of this structure that can yield good approximate numerical values.

The case of extreme value statistics in intermittent chaos is taken up in Section 4. Many of the features found in Section 3 apply to this case as well, with one notable exception: owing to the presence of a marginally stable fixed point at the lower boundary, the probability mass in the entire range from this boundary to the unstable fixed point of the map is depleted very slowly, being $O(n^{-1})$ after n time units as opposed to the typically exponential decay found in fully developed chaos.

In Section 5 a series of results concerning other extremal properties, such as distribution of local maxima, are compiled. It is shown that such properties are even more sensitive to the deterministic origin of the dynamics than the extreme value distribution. Finally, the relevance of the results, comparison with experimental data, and some suggestions for further study are discussed in Section 6.

2. GENERAL FORMULATION

In what follows we shall derive the probability distributions of extremes generated by one-dimensional endomorphisms of the form

$$X_{n+1} = f(X_n, \mu), \qquad X \in [a, b] \tag{2.1}$$

In particular, we shall be interested in values of the control parameter μ for which the dynamics is chaotic.

Let $\rho(X_0)$ be the invariant distribution of the system. The n-time probability density that the $n-1$ values of the record following the state X_0 are $X_1, \ldots, X_{n-1}$, respectively, is

$$\begin{aligned} &\rho_n(X_0, X_1, \ldots, X_{n-1}) \\ &\quad = \rho(X_0)\, \delta(X_1 - f(X_0)) \cdots \delta(X_{n-1} - f^{(n-1)}(X_0)) \end{aligned} \tag{2.2}$$

where the delta functions account for the deterministic character of the dynamics. The cumulative probability for the extreme value in the sequence $X_0, \ldots, X_{n-1}$ is then

$$\begin{aligned} F_n(x) &= \text{Prob}(X_0 \leqslant x, \ldots, X_{n-1} \leqslant x) \\ &= \int_a^x dX_0 \cdots \int_a^x dX_{n-1}\, \rho_n(X_0, \ldots, X_{n-1}) \end{aligned} \tag{2.3}$$

or, using the well-known representation of the delta function,

$$F_n(x) = \int_a^x dX_0\, \rho(X_0) \prod_{m=1}^{n-1} \theta(x - f^{(m)}(X_0)) \tag{2.4}$$

where θ is the Heaviside step function. For $x = b$ all these functions will "fire" giving a contribution equal to unity. This leaves us with the norm of $\rho(X_0)$ leading, as required, to $F_n(b) = 1$.

The density function $\rho_n(x)$ associated to $F_n(x)$ is obtained by differentiating both sides of Eq. (2.4) with respect to x,

$$\begin{aligned} \rho_n(x) = \rho(x) &\prod_{m=1}^{n-1} \theta(x - f^{(m)}(x)) \\ &+ \int_a^x dX_0\, \rho(X_0) \sum_{m=1}^{n-1} \prod_{\substack{k=1 \\ k \neq m}}^{n-1} \delta(x - f^{(m)}(X_0))\, \theta(x - f^{(k)}(X_0)) \end{aligned} \tag{2.5}$$

or, performing formally the integration using the delta function,

$$\rho_n(x) = \rho(x) \prod_{m=1}^{n-1} \theta(x - f^{(m)}(x)) + \sum_{m=1}^{n-1} \sum_{\alpha_m} \frac{\rho(x_{\alpha_m})}{|f^{(m)'}(x_{\alpha_m})|} \theta(x - x_{\alpha_m}) \prod_{\substack{k=1 \\ k \neq m}}^{n-1} \theta(x - f^{(k)}(x_{\alpha_m})) \tag{2.6a}$$

where the prime denotes differentiation and $\{x_{\alpha_m}\}$ are the preimages of the mth iterate of the map f,

$$f^{(m)}(x_{\alpha_m}) = x \tag{2.6b}$$

At the upper boundary $x = b$, Eq. (2.6a) yields

$$\rho_n(b) = \rho(b) + \sum_{m=1}^{n-1} \sum_{\alpha_m} \frac{\rho(b_{\alpha_m})}{|f^{(m)'}(b_{\alpha_m})|} \tag{2.7}$$

where $f^{(m)}(b_{\alpha_m}) = b$.

Equation (2.6a) shows that $\rho_n(x)$ possesses discontinuities on a set of points for which at least one of the Heaviside functions vanishes, namely, at the points

$$\begin{aligned} f^{(m)}(\bar{x}_j) &= \bar{x}_j, \qquad m = 1,..., n-1 \\ f^{(k)}(f^{(-m)}(\bar{x}_j)) &= \bar{x}_j, \qquad m = 1,..., n-1 \quad \text{and} \quad k = 0,..., n-1 \end{aligned} \tag{2.8}$$

This set is nothing but the set of periodic points of all periods up to $n-1$ of the recurrence law, Eq. (2.1). For typical recurrences giving rise to chaotic dynamics it is a dense set in the limit $n \to \infty$, and within each interval delimited by two successive points $\rho_n(x)$ is a smooth function of the same class as $\rho(x)$. Notice that $\rho_n(x)$ is not monotonic: differentiating formally Eq. (2.6a) with respect to x, one obtains a series of contributions weighted by the derivative of the function $f(x)$ or iterates thereof, whose signs alternate according as one is in an ascending or descending branch of the map concerned. We may refer to a function of the kind just described as a *generalized devil's staircase*, in analogy with the more familiar devil's staircase arising in the study of phase locking in the circle map.[10] On the other hand, the corresponding cumulative distribution, Eq. (2.4), will be monotonic, since all terms in Eq. (2.6a) are nonnegative. It will be nondifferentiable at the discontinuity points of $\rho_n(x)$.

The above features show already that the extreme value distributions in chaotic dynamics are very different from those familiar in statistical theory, Eq. (1.2), since, for one thing, these latter distributions are, typically,

smooth functions of x. A more detailed study, performed in Sections 3 and 4, will provide further qualitative and quantitative information on the nature and extent of the difference.

A detailed evaluation of the distributions $F_n(x)$ and $\rho_n(x)$ requires knowledge of the iterative function f. In Sections 3 and 4 such an evaluation will be carried out on two representative classes of chaotic dynamics: fully developed chaos and intermittent chaos.

3. FULLY DEVELOPED CHAOS

We now turn to the application of the foregoing formalism to maps of the unit interval that exhibit fully developed chaos. Throughout this section we use the Bernoulli shift $f(X_0) = 2X_0 \bmod 1$ (which has a discontinuity), the tent map $f(X_0) = 1 - |1 - 2X_0|$ (which has a nondifferentiable point), and the logistic map $f(X_0) = 4X_0(1 - X_0)$ as representative examples.

3.1. $F_n(x)$ for Small Vaues of n

Figures 1–3 display the results for $F_n(x)$ for these maps obtained by numerical simulation in the small-n cases $n = 2$, 3, and 5. The piecewise analytic nature of $F_n(x)$ is clearly evident in each case. Now, the invariant densities for the above-mentioned maps are 1, 1, and $1/\pi[x(1-x)]^{1/2}$, respectively. Had the variables $(X_0, \ldots, X_{n-1})$ been iidrv's, therefore, $F_n(x)$ would have been given by the smooth functions

$$F_n(x) = x^n \qquad \text{(Bernoulli, tent maps)} \tag{3.1}$$

and

$$F_n(x) = [(2/\pi) \sin^{-1} \sqrt{x}]^n \qquad \text{(logistic map)} \tag{3.2}$$

respectively. As the time autocorrelation function $\langle (X_0 - \langle X \rangle)(X_j - \langle X \rangle) \rangle$ is proportional to $\delta_{j,0}$ in each of the three cases under consideration,[11,12] one might imagine that the corresponding extreme value distributions would also be given by the iidrv expressions of Eqs. (3.1)–(3.2). However, a δ-function autocorrelation does not necessarily imply a factorization of joint probability distributions. In short, the signature of the deterministic dynamics is indeed quite pronounced in the extreme value distributions—in both its quantitative and qualitative aspects for small n, and at least qualitatively for larger values of n.

The actual expression for $F_n(x)$ for small values of n can be evaluated directly from the general formula of Section 2, or, equivalently, with the

help of a geometrical construction to be described shortly. For the tent map, we find the piecewise linear expressions

$$F_2(x) = \begin{cases} \dfrac{x}{2}, & 0 \leqslant x \leqslant \dfrac{2}{3} \\ 2x - 1, & \dfrac{2}{3} \leqslant x \leqslant 1 \end{cases} \tag{3.3}$$

$$F_3(x) = \begin{cases} \dfrac{x}{4}, & 0 \leqslant x \leqslant \dfrac{2}{3} \\ \dfrac{7x-4}{4}, & \dfrac{2}{3} \leqslant x \leqslant \dfrac{4}{5} \\ 3x - 2, & \dfrac{4}{5} \leqslant x \leqslant 1 \end{cases} \tag{3.4}$$

These are precisely the functions found by numerical experiment; cf. Figs. 1–3. The nonmonotonic behavior of the slope of $F_n(x)$ [i.e., the density $\rho_n(x)$] for $n \geqslant 3$ should be noted.

Likewise, for the logistic map (which has a fixed point at 3/4) we find the piecewise analytic function

$$F_2(x) = \begin{cases} \dfrac{1}{\pi} \sin^{-1} \sqrt{x}, & 0 \leqslant x \leqslant \dfrac{3}{4} \\ \dfrac{4}{\pi} \sin^{-1} \sqrt{x} - 1, & \dfrac{3}{4} \leqslant x \leqslant 1 \end{cases} \tag{3.5}$$

The slope $\rho_n(x)$ is infinite at both $x = 0$ and $x = 1$. Similarly, $F_3(x)$ in this case is found to be made up of three smooth functions, with breaks in the slope occurring at 3/4 and $(5 + \sqrt{5})/8$ (the largest fixed point of the iterated map $f^{(2)}$), respectively.

In the remaining part of this section we shall use the tent map for a case study in detail. The evaluation of the integral formula (2.4) for $F_n(x)$ with its θ-function constraints may be interpreted graphically as follows. In Fig. 4 we have sketched the maps $f^{(0)}$ through $f^{(3)}$, corresponding to the case $n = 4$, i.e., the maps relevant to the evaluation of $F_4(x)$. For any given value of x in $[0, 1]$, $F_4(x)$ is obtained by integrating $\rho(X_0)$ over those intervals of X_0 in which $x \geqslant \{f(X_0), f^{(2)}(X_0), f^{(3)}(X_0)\}$. Representing the value of x by a horizontal line at a height x above the X_0 axis on the left of the bisectrix $x = X_0$, the range of integration is over those graphs in which there are no segments of map functions between the horizontal line and the "roof" at 1. The possible ranges for different values of x are

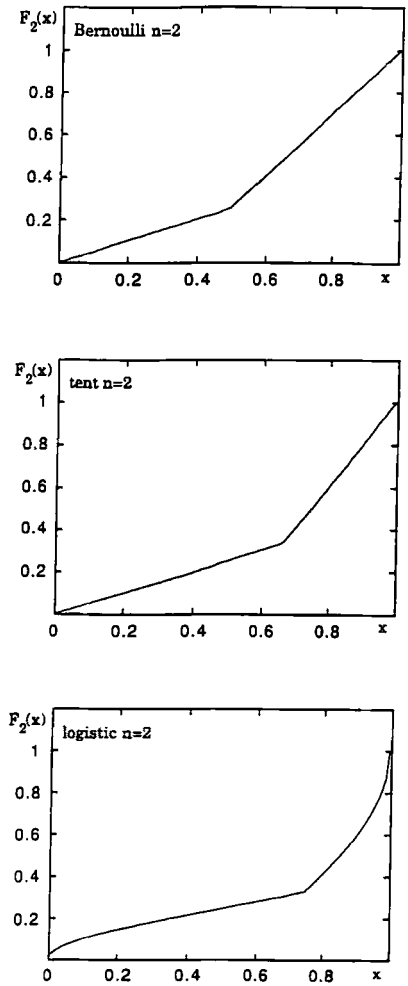

Fig. 1. Cumulative probability distribution for the extreme value $F_2(x)$ for the Bernoulli, tent, and logistic maps deduced numerically using 100,000 realizations and a mesh size $\Delta x = 0.01$.

indicated by dark lines in Fig. 4. As $\rho(X_0) = 1$ in this case, $F_n(x)$ is simply given by the total length of such ranges for any given x. [We have seen in Section 2 that, in general, $F_n(x)$ is piecewise linear whenever $\rho(X_0) = \text{const}$, and piecewise analytic for maps with a smooth invariant density.] A discontinuous *increase* in $\rho_n(x)$ occurs whenever a new contribution (or a *sum* of such contributions) is added to $F_n(x)$ as x increases past a critical value

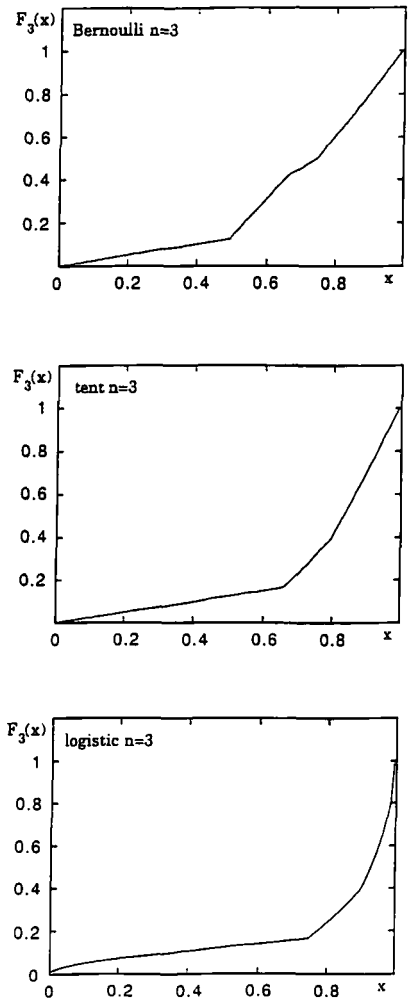

Fig. 2. As in Fig. 1, but for $F_3(x)$.

such as 2/3 or 4/5 or 8/9 in Fig. 4. On the other hand, the rate of increase of $F_n(x)$ *drops* as x crosses a critical value like 6/7 in Fig. 4, i.e., $\rho_n(x)$ *decreases* discontinuously at such a value of x.

Both types of crossings occur at x values corresponding to a fixed point of $f(x)$ or iterates thereof. In Fig. 4 they are depicted as intersections of $f = f^{(1)}, f^{(2)}$, and $f^{(3)}$ with the bisectrix. We notice, however, that for the same value of x, simultaneous intersections (not at fixed points) among the

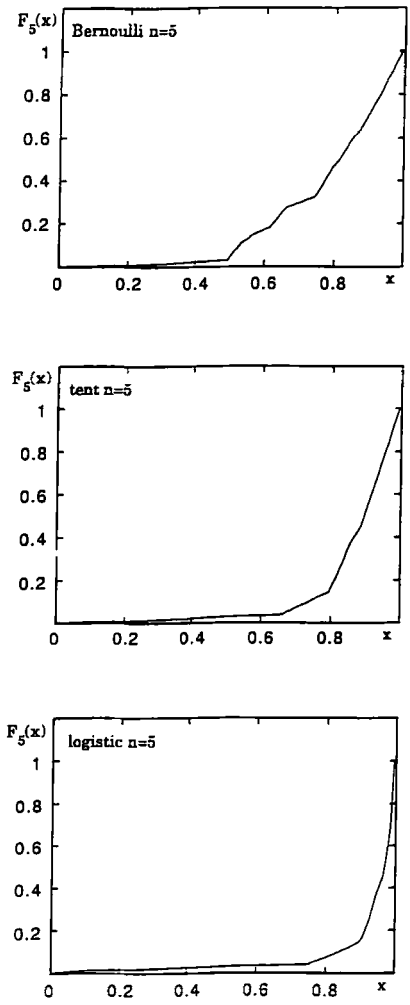

Fig. 3. As in Figs. 1 and 2, but for $F_5(x)$.

higher iterates of f occur to the left of the bisectrix. For example, at $x = 2/3$ the iterates $f^{(2)}$ and $f^{(3)}$ intersect at $X_0 = 1/6$, etc. Intersections of the first type, where a new "valley" opens up, will be referred to as R-type intersections; and those of the second type, where a change of slope of the lines delimiting a valley occurs, will be referred to as L-type intersections. It is important to note that at a given critical value of x all the intersections are

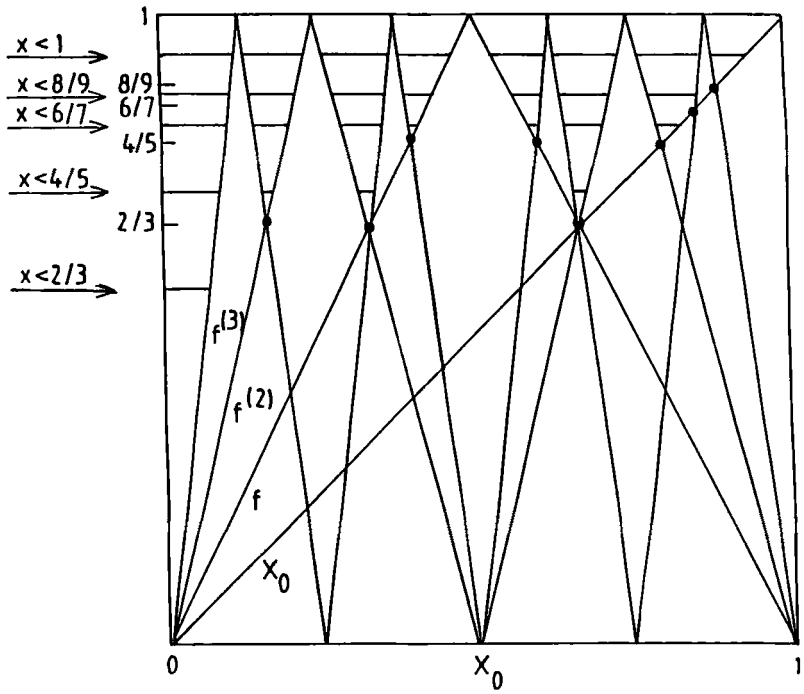

Fig. 4. Maps $f^{(0)}$ to $f^{(3)}$ involved in the evaluation of $F_4(x)$ for the tent map.

necessarily of the same type, either R or L. This explains why the continuous, monotonically increasing function $F_n(x)$ has a steplike behavior, owing to the temporary drop in slope at each L-type intersection.

3.2. Larger n: Initial Stages and Growth of $F_n(x)$ with x

Let us now consider a general, large value of n. It is immediately evident that the initial segment of $F_n(x)$ arises from a single "gap" and is given by

$$F_n(x) = \int_0^{x/2^{n-1}} dX_0 = \frac{x}{2^{n-1}}, \qquad 0 \leqslant x \leqslant \frac{2}{3} \tag{3.6}$$

with $x = 2/3$ being the fixed point of the map. As x increases past this value, $n-1$ additional gaps of equal length open up, and this situation persists till x reaches the value 4/5, the largest fixed point of the once-iterated

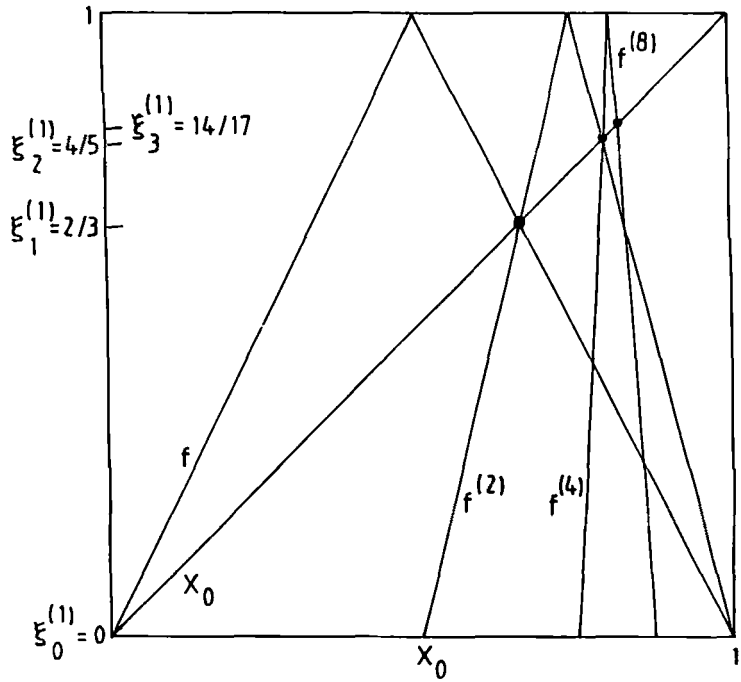

Fig. 5. Sequence of multiple intersections at $\{\xi_k^{(1)}\}=(0, 2/3, 4/5, 14/17,\ldots)$.

map $f^{(2)}$. The length of each of these new gaps is that between the lines $2^{n-2}X_0$ and $2-2^{n-1}X_0$ at ordinate value x. This yields

$$F_n(x)=\frac{(3n-2)\,x-2(n-1)}{2^{n-1}}, \qquad \frac{2}{3}\leqslant x\leqslant\frac{4}{5} \tag{3.7}$$

One might imagine, based on Fig. 4 (which corresponds to the case $n=4$), that a simple R-type intersection [of the level line x, the bisectrix, and a branch of $f^{(2)}(X_0)$] occurs at the value 4/5. However, this is not true for $n\geqslant 9$, because 4/5 is also a fixed point of $f^{(8)}$. The next fixed point of $f^{(8)}$ occurs at 14/17, which is also a fixed point of $f^{(16)}$, and so on. The picture that emerges is sketched in Fig. 5. One therefore has successive "multiple" R-type intersections at values of x given by the infinite sequence

$$\xi_0^{(1)}=0, \quad \xi_1^{(1)}=\tfrac{2}{3}, \quad \xi_2^{(1)}=\tfrac{4}{5}, \quad \xi_3^{(1)}=\tfrac{14}{17}, \quad \xi_4^{(1)}=\tfrac{212}{257},\ldots \tag{3.8}$$

[the reason for the superscript (1) will become clear shortly]. From the geometry of Fig. 5, we can deduce the recursion relation for the points $\xi_k^{(1)}$:

$$\xi_k^{(1)} = \frac{(2^{2^{k-1}} - 1)\,\xi_{k-1}^{(1)} + 2}{2^{2^{k-1}} + 1}, \qquad k \geqslant 1 \tag{3.9}$$

where $\xi_0^{(1)} = 0$. The explicit solution is

$$\xi_k^{(1)} = 1 - (2^{2^k} - 1)^{-1} \prod_{l=0}^{k-1} (2^{2^l} - 1) \tag{3.10}$$

which converges extremely rapidly (superexponentially!) to the limiting value $\xi_\infty^{(1)} = 0.824908...$ (which is less than 6/7). Therefore, for any given sufficiently large n, the slopes of the successive segments of $F_n(x)$ *increase* in jumps with increasing x, at least until $x = \xi_q^{(1)}$, where $q = 1 + [\log_2(n-1)]$, $[\cdot]$ standing for "the largest integer in." However, the probability mass in this range of x remains exponentially small for very large values of n, because the contribution from each gap is bounded from above by $1/2^{n-1}$, the multiplicity of new gaps at each $\xi_k^{(1)}$ increases no faster than a power of n, and the sequence covers an extremely short range of x beyond the first few points.

Similar sequences of "multiple" R-type intersections occur at higher values of x, beyond $\xi_\infty^{(1)}$. The next such sequence is determined by common fixed points of $f^{(3)}, f^{(6)}, f^{(12)}, ...$ *ad infinitum*, given by the recursion relation

$$\xi_k^{(3)} = \frac{(2^{3\cdot 2^{k-1}} - 1)\,\xi_{k-1}^{(3)} + 2}{2^{3\cdot 2^{k-1}} + 1}, \qquad k \geqslant 1 \tag{3.11}$$

with $\xi_0^{(3)} = 6/7$. Thus $\xi_1^{(3)} = 8/9$, $\xi_2^{(3)} = 58/65$, and so on. This sequence converges even more rapidly than that of Eq. (3.10), to the value $\xi_\infty^{(3)} = 0.892360...$. Such sequences $\xi_k^{(p)}$ exist for all odd integers p, and as $n \to \infty$, more and more of them begin to occur: the general recursion relation for these points is

$$\xi_k^{(p)} = \frac{(2^{p\cdot 2^{k-1}} - 1)\,\xi_{k-1}^{(p)} + 2}{2^{p\cdot 2^{k-1}} + 1} \tag{3.12}$$

where $p = 1, 3, 5, ...$ and $k = 1, 2, ...$ for each p. [This explains the notation $\xi_k^{(1)}$ used earlier for the original sequence in Eqs. (3.8)–(3.10).] The explicit solution to Eq. (3.12) is

$$\begin{aligned} \xi_1^{(p)} &= 1 - (1 - \xi_0^{(p)})(2^p - 1)(2^p + 1)^{-1} \\ \xi_k^{(p)} &= 1 - (1 - \xi_0^{(p)})(2^p - 1)(2^{p\cdot 2^{k-1}} + 1)^{-1} \prod_{l=0}^{k-2} (2^{p\cdot 2^l} - 1), \qquad k \geqslant 2 \end{aligned} \tag{3.13}$$

As p increases, more than one such sequence can occur for a given value of p, but the total span of each sequence decreases extremely rapidly. For a general odd number $p>3$, there are in fact $(2^{p-3}-1)$ distinct sequences, with starting points $\xi_0^{(p)}$ given by $(2^p-2r)/(2^p-1)$, where r runs from 1 to $(2^{p-3}-1)$. Thus for $p=5$, for instance, we have three sequences starting at 26/31, 28/31, and 30/31, respectively. As already mentioned, however, the total probability mass in these sequences is extremely small. Moreover, for a given value of n, any sequence $\{\xi_k^{(p)}\}$ is cut off at

$$k=1+\left[\log_2\frac{n-1}{p}\right]$$

as the highest iterated map involved in $F_n(x)$ is $f^{(n-1)}$.

3.3. Behavior of $F_n(x)$ Very Close to $x=1$

Based on the foregoing, one might be tempted to conclude that the probability mass in $F_n(x)$ is concentrated in an exponentially thin layer [of width perhaps $O(2^{-n})$] near $x=1$, for large values of n. We shall subsequently show that this is not so: in terms of *measure*, the behavior of $F_n(x)$ is quantitatively similar to that of the "statistical" or iidrv expression $[F(x)]^n=x^n$. The latter quantity has a total probability mass $1-(1-n^{-1})^n\approx 1-e^{-1}$ in a layer of width n^{-1} at the upper boundary 1. We shall establish a similar result for $F_n(x)$, as far as the probability mass is concerned. The actual functional structure of $F_n(x)$ is, however, completely different from that of the smooth function $[F(x)]^n$. This aspect will be discussed further in the next subsection. Here we examine $F_n(x)$ in the immediate vicinity of $x=1$.

The general scenario that obtains very close to $x=1$, for large values of n, is shown in Fig. 6. In constructing $F_n(x)$, it turns out to be more convenient to compute increments to the piecewise constant density $\rho_n(x)$ and then use the fact that $F_n(x)$ is continuous. Now $F_n(1)=1$, and Eq. (2.7) applied to the tent map yields $\rho_n(1)=n$. We therefore have immediately

$$F_n(x)=nx-(n-1), \qquad x\in\left[1-\frac{1}{2^{n-1}+1},\,1\right] \tag{3.14}$$

The lower limit in the above range of x follows from the fact that the critical point immediately below 1 is the largest fixed point of $f^{(n-1)}$, i.e., the solution to $2^{n-1}-2^{n-1}X_0=X_0$. Below this value of x, the contribution from the single gap between the lines $2^{n-1}-2^{n-1}X_0$ and X_0 vanishes, and this situation persists until we go down to the next critical point, the

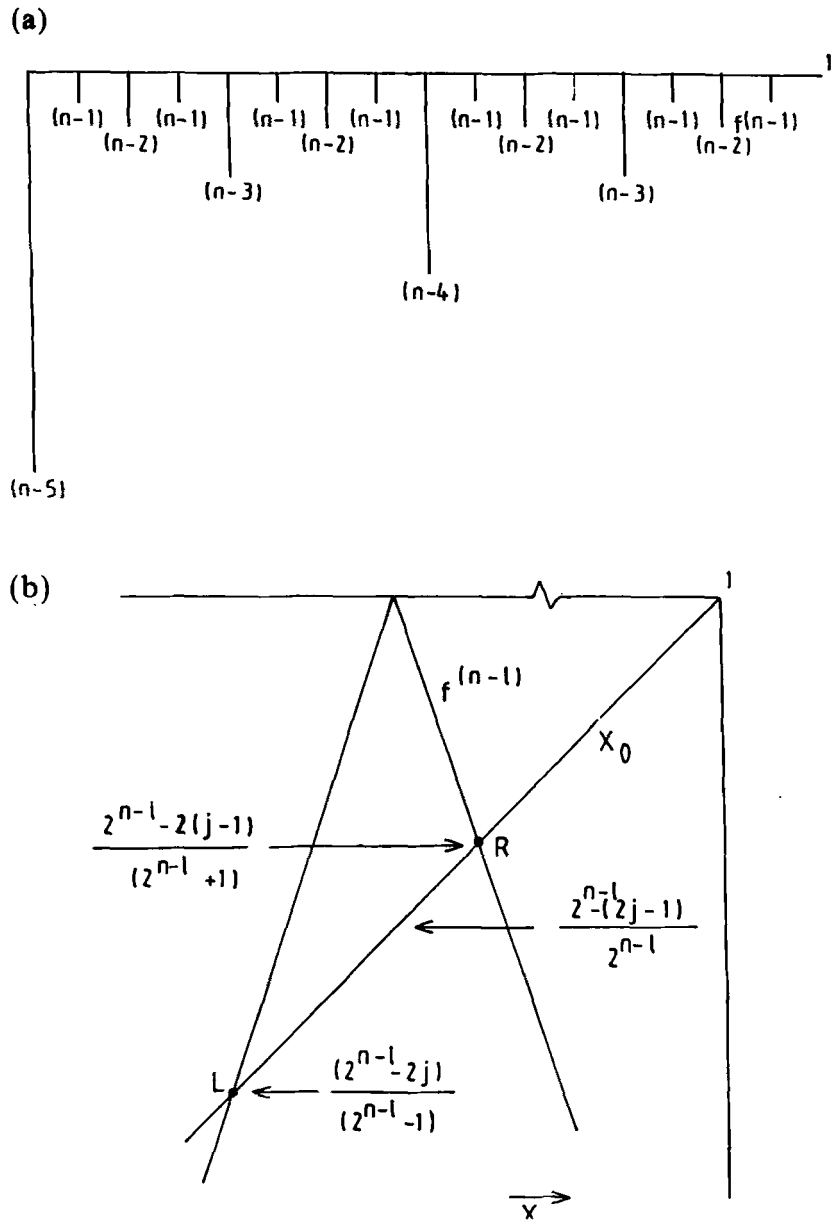

Fig. 6. Scenario close to $x = 1$: (a) hierarchy of peak positions of the iterated maps in the range $1 - \lambda \leqslant x \leqslant 1$; (b) closer up sketch of the L and R intersections associated with the jth peak (counting leftward from 1) of the iterate $f^{(n-1)}$.

penultimate fixed point of $f^{(n-1)}$, given by $2^{n-1}X_0-(2^{n-1}-2)=X_0$. Subtracting this contribution (=the length of the gap) from $nx-(n-1)$, we get

$$F_n(x)=\left(n-1-\frac{1}{2^{n-1}}\right)x-(n-2), \qquad x\in\left[1-\frac{1}{2^{n-1}-1}, 1-\frac{1}{2^{n-1}+1}\right] \tag{3.15}$$

To proceed, it is helpful to note the following. The size of the gap at ordinate level x in the valley formed by the intersection of the lines $c_1-m_1X_0$ and $m_2X_0-c_2$ $(m_1, m_2>0)$ is $(m_1^{-1}+m_2^{-1})x-c_1m_1^{-1}+c_2m_2^{-1}$, so that the increment to $\rho_n(x)$ arising from this gap is just $m_1^{-1}+m_2^{-1}$. In general, therefore, to find the increment to $\rho_n(x)$ at any R-type critical point, we have merely to add up the reciprocals of the magnitudes of the slopes of *all* the lines delimiting the valleys that open up at that critical value x. An obvious modification of this rule applies at L-type intersections.

To deduce the value of $F_n(x)$ immediately below $x=1-(2^{n-1}-1)^{-1}$, we must *subtract* the *three* contributions that open up as x increases past the critical point $1-(2^{n-2}+1)^{-1}$ from below (one from the intersection of $f^{(n-2)}$ with $f^{(0)}$, and two from the intersection of $f^{(n-1)}$ with $f^{(1)}$). The result is

$$F_n(x)=\left(n-\frac{1}{2^{n-2}}\right)x-\left(n-1-\frac{1}{2^{n-2}}\right),$$

$$x\in\left[1-\frac{1}{2^{n-2}+1}, 1-\frac{1}{2^{n-1}-1}\right] \tag{3.16}$$

Similarly, in the next range we find

$$F_n(x)=\left(n-2-\frac{1}{2^{n-2}}-\frac{1}{2^{n-3}}\right)x-\left(n-3-\frac{1}{2^{n-2}}\right),$$

$$x\in\left[1-\frac{1}{2^{n-2}-1}, 1-\frac{1}{2^{n-2}+1}\right] \tag{3.17}$$

and so on. The up-and-down variation of the slope $\rho_n(x)$ is immediately evident from these results.

In principle, we could go on in this fashion to ranges of x farther and farther away from $x=1$. Our interest, however, is in identifying the extent of the layer near $x=1$ supporting the bulk of the probability mass. This is done in the next subsection.

3.4. Probability Mass in the Layer $1-n^{-1} \leqslant x \leqslant 1$

To a very good approximation, the layer of width of order n^{-1} just below 1 can be modeled as in Fig. 6: successive L- and R-type intersections of the bisectrix by a hierarchical arrangement of the highest iterates $f^{(n-1)}$, $f^{(n-2)}$,... that occur in $F_n(x)$. The basic interval between successive peaks of the maps at ordinate 1 is 2^{1-n}. Let us consider a range $[1-\lambda, 1]$ of x, and for definiteness choose λ such that it is just larger that $2^{\kappa-n}$, so that there is a single peak of $f^{(n-\kappa)}$ just to the right of $1-\lambda$. Then $\kappa=[n-\log_2 n]$ ensures that $\lambda \approx n^{-1}$. The problem of finding $F_n(x)$ is now that of counting the number of L- and R-type intersections on the bisectrix and the number of simultaneous intersections occurring to the left of the bisectrix for each of these, and then adding up all the contributions.

The calculation is greatly facilitated by two lemmas.

Lemma 1. At an R-type intersection of $f^{(n-l)}$ with the bisectrix at the point ξ_R, the increase in the density $\rho_n(x)$ is given by

$$\rho_n(x=\xi_R+0)-\rho_n(x=\xi_R-0)=l(1+2^{l-n}) \tag{3.18}$$

Similarly, at an L-type intersection of $f^{(n-l)}$ at ξ_L, the change in $\rho_n(x)$ is given by

$$\rho_n(x=\xi_L+0)-\rho_n(x=\xi_L-0)=-l(1-2^{l-n}) \tag{3.19}$$

To prove this, we have only to note that at the level $x=\xi_R$ (or ξ_L), we have simultaneously one intersection between $f^{(n-l)}$ and $f^{(0)}$, two intersections between $f^{(n-l+1)}$ and $f^{(1)}$, 2^2 between $f^{(n-l+2)}$ and $f^{(2)}$,..., 2^{l-1} between $f^{(n-1)}$ and $f^{(l-1)}$. Therefore, using our earlier observation [made below Eq. (3.15)] on the increment of $\rho_n(x)$ at an intersection between two lines, we have

$$\rho_n(x=\xi_R+0)-\rho_n(x=\xi_R-0)=\sum_{m=0}^{l-1} 2^m\left(\frac{1}{2^{n-l+m}}+\frac{1}{2^m}\right) \tag{3.20}$$

and

$$\rho_n(x=\xi_L+0)-\rho_n(x=\xi_L-0)=\sum_{m=0}^{l-1} 2^m\left(\frac{1}{2^{n-l+m}}-\frac{1}{2^m}\right) \tag{3.21}$$

from which Eqs. (3.18) and (3.19) follow at once.

The second lemma gives the change in $F_n(x)$ itself. Now, the jth peak of $f^{(n-l)}(X_0)$ (counting leftward from 1) occurs at $X_0=1-(2j-1)/2^{n-l}$.

The L- and R-type intersections of the ascending and descending branches of $f^{(n-l)}$ associated with this peak occur at $\xi_L = 1-(2j-1)/(2^{n-l}-1)$ and $\xi_R = 1-(2j-1)/(2^{n-l}+1)$ respectively. We then have the following result.

Lemma 2. If $F_n(x) = mx + c$ just above $x = \xi_R$, then

$$F_n(x) = mx + c + \frac{(1-x)\,l}{2^{n-l-1}} \tag{3.22}$$

just below $x = \xi_L$.

To prove this, we have merely to use Eqs. (3.20) and (3.21) and the continuity of $F_n(x)$ at ξ_R and ξ_L. It is noteworthy that there is no dependence on j, the label of the peak of $f^{(n-l)}$, in Eq. (3.22). This is not true, for instance, for $F_n(x)$ in the intermediate region $\xi_L < x < \xi_R$.

With the help of Eq. (3.22), we are finally ready to reconstruct $F_n(x)$ at $x = 1-\lambda$. In this region we have $2^{\kappa-l-1}$ peaks of $f^{(n-l)}$, where l runs from 1 to $\kappa-1$, and a final peak of $f^{(n-\kappa)}$. Therefore, setting $\lambda = n^{-1}$, or $\kappa \approx n - \log_2 n$, and using Eqs. (3.14) and (3.22), we get

$$\begin{aligned} F_n(1-n^{-1}) &\simeq nx - (n-1) + (1-x)\left[\frac{\kappa}{2^{n-\kappa-1}} + \sum_{l=1}^{\kappa-1} 2^{\kappa-l-1}\,\frac{l}{2^{n-l-1}}\right] \\ &\simeq \frac{(n-\log_2 n)(n-\log_2 n+3)}{2n^2} \end{aligned} \tag{3.23}$$

This is quite comparable to, although a bit larger than, the value $(1-n^{-1})^n$ ($\to e^{-1}$ as $n \to \infty$) that obtains for iidrv's. We note, however, that Eq. (3.23) is an overestimate, as we have replaced the smaller actual contributions from those multiple intersection sequences $\{\xi_k^{(p)}\}$ that occur in the region $1-\lambda \leqslant x \leqslant 1$ by somewhat larger ones from simple L- and R-type intersections.

Figures 7 and 8 depict the results of numerical experiments for a moderately large value of n ($= 100$) that corroborate our theoretical conclusions regarding the behavior of $\rho_n(x)$ and $F_n(x)$. The up-and-down steplike form of $\rho_n(x)$ is strikingly evident, in contrast to the iidrv prediction $nx^{n-1} = 100x^{99}$. Although integration makes this behavior somewhat smoother, $F_n(x)$ is still qualitatively quite different from the iidrv distribution x^n. It is clear from our theoretical analysis and the actual numerical experiment that these differences will persist even if n becomes very large, and that in the layer of width $O(n^{-1})$ about 1 the scenario depicted in Figs. 7 and 8 will continue to be valid for any value of n. It is only in the *final, exponentially small* range of x of order 2^{-n} {to be precise, in $[1-(2^{n-1}+1)^{-1}, 1]$} that the exact expression for $F_n(x)$, namely $nx - n + 1$, coincides with the leading behavior of x^n in the limit $x \to 1$.

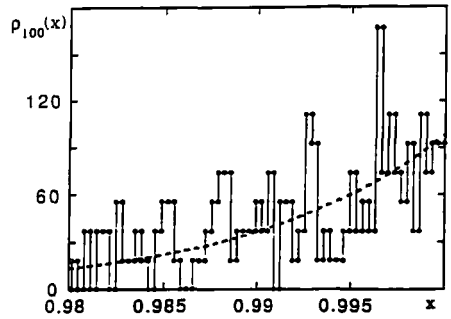

Fig. 7. Probability density for the extreme value $\rho_n(x)$, $n = 100$, for the tent map in the range $0.98 \leqslant x \leqslant 1$ deduced numerically using 100,000 realizations. The size of the bin used is $\Delta x = 3.33 \times 10^{-4}$. The dashed line represents the iidrv prediction, $100x^{99}$.

As mentioned in the Introduction, the most important classical result for iidrv's (and even for correlated random variables, under fairly general conditions) is the existence of just three universality classes of limiting distributions for linearly rescaled variables. For the tent map under consideration, and also for the Bernoulli map, the probability distribution $[F(x)]^n = x^n$ falls, via the rescaling $a_n = n^{-1}$ and shift $b_n = 1 - n^{-1}$, into the domain of attraction of the limiting distribution

$$H_1(x) = \lim_{n \to \infty} (n^{-1}x + 1 - n^{-1})^n = \exp(x - 1), \qquad x \leqslant 1 \tag{3.24}$$

Similarly, the classical theory for iidrv's shows[6] that the distribution $[F(x)]^n$ in the case of the logistic map, Eq. (3.1b), tends to the limiting distribution $\exp[-(1-x)^{1/2}]$ for rescaled variables. However, the piecewise analytic nature of the correct $F_n(x)$, with breaks in the slope at a dense set

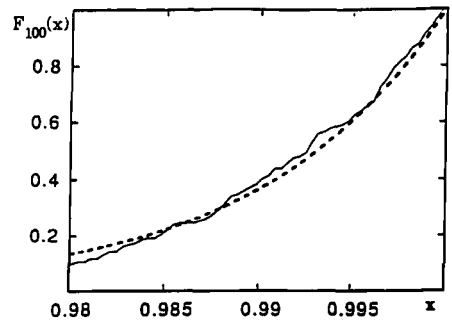

Fig. 8. As in Fig. 7, but for the cumulative probability distribution, $F_{100}(x)$. The dashed line represents the iidrv prediction x^{100}.

of points as $n \to \infty$, precludes the possibility of the existence of such simple limiting extreme value distributions, under linear rescaling, of sequences generated by chaotic dynamics.

4. INTERMITTENT CHAOS

Next, we turn to extreme value statistics in the case of intermittent chaos. Specifically, we consider the example of the square root cusp map $f(X_0) = 1 - 2|X_0|^{1/2}$, $X_0 \in [-1, 1]$, with invariant density[13] $\rho(x) = (1-x)/2$ and corresponding cumulative probability $F(x) = (1+x)(3-x)/4 = 1 - \rho^2(x)$. The rapid shrinking (owing to the cusp) of the window about $X_0 = 0$ that is injected into the vicinity of the marginally stable fixed point at $X_0 = -1$ in two iterations, the slowing down associated with the latter, and the existence of a nontrivial, slowly decreasing time autocorrelation function[12,13] may be expected to produce some new features in $F_n(x)$. For ready reference we note that, if $(X_0, \ldots, X_{n-1})$ had been iidrv's, $F_n(x)$ would

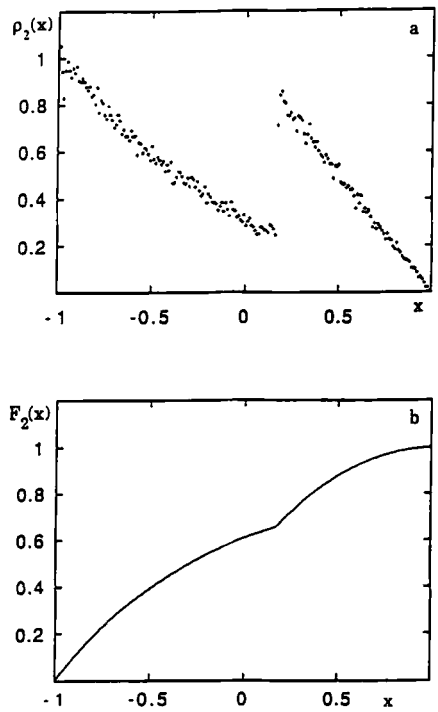

Fig. 9. (a) Extreme value probability density and (b) cumulative probability distribution, for $n = 2$ for the cusp map as deduced from numerical simulation using 100,000 realizations and a mesh size of $\Delta x = 0.001$.

have been $[F(x)]^n = [1-\rho^2(x)]^n$ in this instance. The corresponding classical limiting distribution for rescaled variables would have been $\exp[-(1-x)^2]$.

4.1. $F_n(x)$ for Small n

The distribution $F_2(x)$ is easily calculated, and is given by

$$F_2(x) = \begin{cases} \frac{3}{4} - \frac{1}{2}\rho^2(x) - \frac{1}{4}\rho^4(x), & 0 \leqslant x \leqslant 3-2\sqrt{2} \\ 1-2\rho^2(x), & 3-2\sqrt{2} \leqslant x \leqslant 1 \end{cases} \tag{4.1}$$

where, as already mentioned, $\rho(x) = (1-x)/2$, and $3-2\sqrt{2}$ is the fixed point of the map. Similarly, $F_3(x)$ has two breaks in slope, and so on. Figures 9 and 10 represent the results of numerical simulation for $F_2(x)$ and $F_3(x)$ and the corresponding densities $\rho_2(x)$ and $\rho_3(x)$.

We now show that, for arbitrarily large values of n, the behavior of $F_n(x)$ is strongly controlled by the intermittent nature of the map.

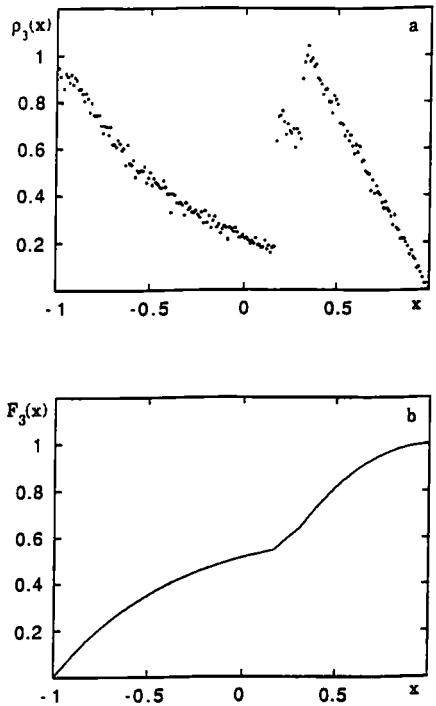

Fig. 10. As in Fig. 9, but for $\rho_3(x)$ and $F_3(x)$.

4.2. Behavior Near $x = 1$

The basic property that we need to note for our present purposes is the following: $|f^{(m)'}(X_0)| = 1$ at $X_0 = \pm 1$ for *all* $m \geqslant 1$. This means that the branches of the iterates $f^{(m)}(X_0)$ become extremely steep as m gets larger, because the positions of the peaks (and hence the fixed points, too) only move very slowly toward the ends ± 1. It is this relatively slow rate of convergence that is crucial.

Let $(-1 + 4u_m,\ 1 - 4u_m)$ be the values of X_0 at which the first and last peaks of $f^{(m)}(X_0)$ occur. It is then easy to show that $u_{m+1} = u_m(1 - u_m)$, with $u_1 = 1/4$. This is just the logistic map at parameter value 1, at which the fixed point $u_\infty = 0$ becomes marginally stable (this is the reason for the slow convergence of the sequence u_m). The asymptotic behavior of u_m is[14]

$$u_m = m^{-1} + O(m^{-2} \log m) \tag{4.2}$$

Moreover, the position of the final zero of $f^{(m)}$ is also that of the last peak of $f^{(m+1)}$. These facts imply that, when n is large, the last fixed point x^* of $f^{(m-1)}(X_0)$ satisfies

$$1 - \frac{4}{n-1} < x^* < 1 - \frac{4}{n} \tag{4.3}$$

The final segment of the piecewise analytic function $F_n(x)$ obtains in the range $x^* \leqslant x \leqslant 1$, which is, by (4.3), a layer of width of order n^{-1}. Since $\rho(1) = 0$ and the slope of any $f^{(m)}$ at every preimage of 1 is infinite, Eq. (2.7) yields $\rho_n(1) = 0$ for every n. Very close to $x = 1$, Eq. (2.5) gives the leading behavior

$$\begin{aligned} \rho_n(x) &= \rho(x) + \int_{-1}^{1} dX_0\, \rho(X_0) \sum_{m=1}^{n-1} \delta(x - f^{(m)}(X_0)) \\ &= n\rho(x) \end{aligned} \tag{4.4}$$

on setting $x = 1$ in the θ-functions and using the Frobenius–Perron equation for the invariant density $\rho(x)$. Integrating this result, we have

$$F_n(x) \approx 1 - n\rho^2(x) \tag{4.5}$$

in this final range of x. Figures 11a and 11b show the results of a numerical experiment on extreme value statistics in the cusp map for $n = 100$. These results, and similar ones for other values of n, are in close agreement with the theoretical predictions derived above.

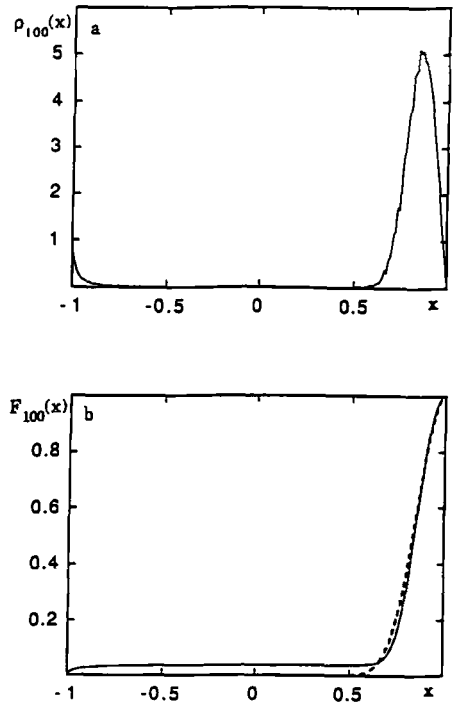

Fig. 11. As in Fig. 10, but for $\rho_{100}(x)$ and $F_{100}(x)$. The dashed line represents the iidrv prediction $[1-\rho^2(x)]^{100}$.

4.3. Behavior Near $x=-1$

Since $F(x)=(1+x)(3-x)/4$, the iidrv expression $[F(x)]^n$ would imply a very rapid vanishing [like $(1+x)^{n-1}$] of the corresponding probability density as $x\to -1$. In reality, however, since $|f^{(m)'}(-1)|=1$ for every iterate of the map, we find a totally different behavior. For $0\leqslant x\leqslant 3-2\sqrt{2}$, $F_n(x)$ is given by

$$F_n(x)=\int_{-1}^{-1+\omega_{n-1}(x)} dX_0\,\rho(X_0) \tag{4.6}$$

where $-1+\omega_{n-1}(x)$ is the smallest root of the equation $f^{(n-1)}(X_0)=x$, i.e., of the equation

$$1-2[2[\cdots[2(-X_0)^{1/2}-1]^{1/2}\cdots]^{1/2}-1]^{1/2}=x \tag{4.7}$$

To leading order in $(1+x)$, this yields $\omega_{n-1}(x) = (1+x)$. Therefore from Eq. (4.6) we find the leading behavior

and
$$F_n(x) = 1 + x \tag{4.8}$$

$$\rho_n(x) = 1 \tag{4.9}$$

as $x \to -1$, for *all* n. A comparison of Figs. 9 and 10 ($n = 2, 3$) and Fig. 11 ($n = 100$) shows that the density $\rho_n(x)$ drops rapidly to practically zero from its initial value of unity as x moves out from -1, particularly for large values of n. It begins to rise again only beyond the fixed point, very slowly at first, and then ever more rapidly. In reality this is not a smooth rise, but rather a series of jumps or serrations at the points of non-analyticity of $F_n(x)$, as is clear from Fig. 12a.

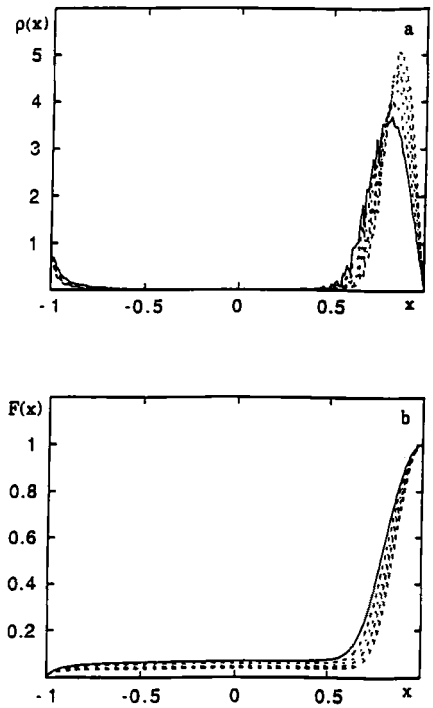

Fig. 12. (a) Density $\rho_n(x)$ and (b) cumulative probability distribution $F_n(x)$ for $n = 50$ (solid line), 60, 70, 80, 90, and 100 (broken lines). Note the serrations in $\rho_n(x)$ in its "ascending" range and the slow decrease of the plateau value of $F_n(x)$ with increasing n.

As a consequence of the behavior of $\rho_n(x)$ described above, $F_n(x)$ [which starts out as in Eq. (4.8)] has a long "plateau" region. Its value in the plateau is given by the contribution from the single "gap" between -1 and the first ascending branch of $f^{(n-1)}(X_0)$, and a convenient measure is its value at $x=0$: as we have already mentioned, the first zero of $f^{(n-1)}(X_0)$ is also the position of the leftmost peak of $f^{(n)}(X_0)$. Therefore this position is given, asymptotically, by $X_0 = -1 + 4n^{-1}$, yielding the asymptotic estimate

$$F_n(0) \sim \int_{-1}^{-1+4n^{-1}} dX_0 \frac{1-X_0}{2} \sim 4n^{-1} \tag{4.10}$$

For $n=100$, this is already accurate to within $\sim 8\%$ of the exact value. [In the latter, the factor $n^{-1}=0.01$ in the upper limit of integration in Eq. (4.10) is replaced by 0.009396... .]

This persistent layer of probability mass at the lower end of the range of the variates X_i, which scales (rather slowly) like n^{-1}, is perhaps the most striking feature of the extreme value distribution in the case of intermittent chaos.

5. LOCAL MAXIMA AND OTHER EXTREME VALUES

There are several other extreme value statistics that one could consider in order to identify other possible distinctive signatures of chaotic dynamics. One such statistic that readily comes to mind is the probability of an increasing (or nondecreasing) sequence $\{X_i\}$, i.e., $\Pr(X_0 \leqslant X_1 \cdots \leqslant X_{n-1} \leqslant x) \equiv \Phi_n(x)$. If the $\{X_i\}$ are iidrv's, this distribution would be simply $[F(x)]^n/n!$. In contrast, in the one-dimensional chaotic dynamics we have been considering,

$$\Phi_n(x) = \int_a^x dX_{n-1} \int_a^{X_{n-1}} dX_{n-2} \cdots \int_a^{X_1} dX_0\, \rho(X_0) \prod_{m=1}^{n-1} \delta(X_m - f(X_{m-1}))$$

It is convenient to recast this relation in the form

$$\Phi_n(x) = \int_a^b dX_{n-1} \int_a^b dX_0\, \rho(X_0)\, \theta(x - X_{m-1}) \cdots \theta(X_1 - X_0)$$

$$\times \delta(X_{n-1} - f^{(n-1)}(X_0)) \cdots \delta(X_1 - f(X_0)) \tag{5.1}$$

For symmetric one-humped maps, Eq. (5.1) can be greatly simplified: $\Phi_n(x)$ is piecewise analytic, with just *two* segments. The break in slope occurs at the nontrivial fixed point of the map, $f(\bar{x}) = \bar{x}$. We find

$$\Phi(x) = \int_a^{x_1(x)} dX_0\, \rho(X_0), \qquad a \leqslant x \leqslant \bar{x} \tag{5.2}$$

where $x_1(x)$ is the smallest root of $f^{(n-1)}(X_0) = x$, and

$$\Phi_n(x) = \int_a^{x_1(x)} dX_0\, \rho(X_0) + \int_{x_2(x)}^{\bar{x}_{\min}} dX_0\, \rho(X_0), \qquad \bar{x} \leqslant x \leqslant b \tag{5.3}$$

where $x_2(x)$ is the next root of $f^{(n-1)}(X_0) = x$, and $\bar{x}_{\min}$ is the smallest root of $f^{(n-1)}(X_0) = f^{(n-2)}(X_0)$. Notice the relation $x_2(\bar{x}) = \bar{x}_{\min}$.

Applying the foregoing to the tent map, we get

$$\Phi_n(x) = \begin{cases} \dfrac{x}{2^{n-1}}, & 0 \leqslant x \leqslant \dfrac{2}{3} \\ \dfrac{x - 1/3}{2^{n-2}}, & \dfrac{2}{3} \leqslant x \leqslant 1 \end{cases} \tag{5.4}$$

This is to be compared with the iidrv result $x^n/n!$. In particular, the *total* probability of a nondecreasing sequence of n successive members of the time series is $2^{3-n}/3$ $(n \geqslant 2)$, instead of $1/n!$ (implying an exponential, rather than n^{-n}, falloff with increasing n).

Another important statistic, and one that involves the short-time behavior of the dynamical system, is the distribution of *local maxima*: focusing on any three successive members (X_0, X_1, X_2) of a time sequence, and given that the distribution of X_0 is governed by the invariant density $\rho(X_0)$, what is $\Pr(X_1 \leqslant x \mid X_0,\ X_2 < X_1) \equiv \psi(x)$? This tells us how the local maxima ("spikes") are distributed in the time series.

If the three variables are iidrv's, the above probability distribution is given by

$$\Pr(X_1 \leqslant x \mid X_0 < X_1,\ X_2 < X_1) = \psi(x) = \int_a^x dX_0\, \rho(X_0)\, F^2(X_0) \tag{5.5}$$

yielding $x^3/3$ for the tent map. Coming now to the case of time series generated by deterministic chaos, we first note that a given recurrence law may not permit all possible sequences. For instance, it is easy to see that the tent map does not permit a sequence of the form $X_0 < X_1 < X_2$, $X_2 > X_3 > X_4$. More quantitatively, the exact expression of $\psi(x)$ is

$$\psi(x) = \int_a^x dX_1 \int_a^{X_1} dX_0 \int_a^{X_1} dX_2\, \rho(X_0)\, \delta(X_1 - f(X_0))\, \delta(X_2 - f^{(2)}(X_0)) \tag{5.6}$$

For the class of maps we have been considering, $\psi(x)$ is identically zero in the range $a \leqslant x \leqslant \bar{x}$, where $\bar{x}$ is the nonzero fixed point of the map, as before. Specifically, we find the following results:

- For the Bernoulli shift,

$$\psi(x) = \begin{cases} 0, & 0 \leqslant x \leqslant \frac{1}{2} \\ \dfrac{2x-1}{4}, & \frac{1}{2} \leqslant x \leqslant 1 \end{cases} \tag{5.7}$$

Therefore the total probability is $\psi(1) = 1/4$ rather than 1/3, as one might have imagined at first sight.

- For the tent map,

$$\psi(x) = \begin{cases} 0, & 0 \leqslant x \leqslant \frac{2}{3} \\ x - \frac{2}{3}, & \frac{2}{3} \leqslant x \leqslant 1 \end{cases} \tag{5.8}$$

The total probability is 1/3, as expected.

- For the logistic map,

$$\psi(x) = \begin{cases} 0, & 0 \leqslant x \leqslant \dfrac{3}{4} \\ \dfrac{2}{\pi} \sin^{-1} \sqrt{x} - \dfrac{2}{3}, & \dfrac{3}{4} \leqslant x \leqslant 1 \end{cases} \tag{5.9}$$

The total probability is 1/3, although the interval of integration over X_0, when $x = 1$, runs from 1/4 to 3/4. Weighting with the invariant density reduces $\psi(1)$ from 1/2 to 1/3.

- For the cusp map, which is *not* δ-correlated,

$$\psi(x) = \begin{cases} 0, & -1 \leqslant x \leqslant 3 - 2\sqrt{2} \\ 3 - 2\sqrt{2} - \dfrac{(1-x)^2}{4}, & 3 - 2\sqrt{2} \leqslant x \leqslant 1 \end{cases} \tag{5.10}$$

The total probability is $3 - 2\sqrt{2}$ in this case.

Figures 13a–13c show the results of numerical experiments for the Bernoulli, tent, and cusp maps. They agree with the expressions given above, and are quite different from what would obtain for independent random variables distributed according to $\rho(X_0)$ in each case.

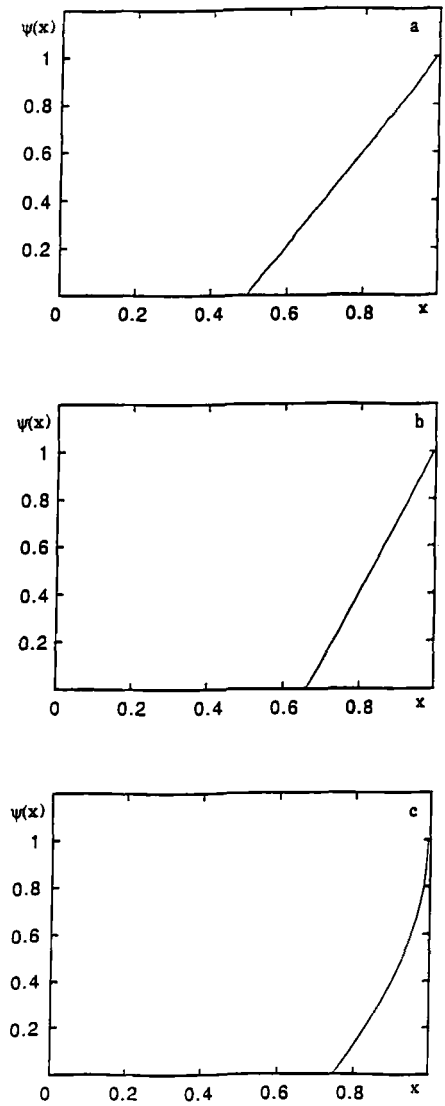

Fig. 13. Normalized distribution $\psi(x)/\psi(1)$ of local maxima by numerical simulation for (a) the Bernoulli, (b) the tent, and (c) the logistic maps deduced numerically using 100,000 realizations and a mesh size $\Delta x = 0.01$.

6. CONCLUDING REMARKS

We have identified a number of qualitative and quantitative features of extreme value distributions generated by chaotic dynamical systems in the regimes of fully developed chaos and of intermittent chaos.

The most important single conclusion from our investigation is that deterministic chaos leaves a clearcut signature in the extreme value properties. First, the cumulative extreme value distributions and their associated densities are, respectively, nondifferentiable and discontinuous on a set of points belonging to the periodic orbits of the system. For short data sets the result is completely different from the distributions derived in the classical statistical theory of extremes. As the number of data tends to infinity the points of nondifferentiability (or of discontinuity in the density) define a dense set: despite an overall resemblance with the statistical distributions of the classical theory, deep differences in structure subsist. The differences become even more radical for such properties as the distribution of local maxima, which actually reflect the short-time properties of the dynamics even for arbitrarily long time series.

The specific examples considered in the present paper have been limited to one-dimensional recurrences. Future investigations in this area should aim at higher-dimensional chaos and, especially, at continuous-time dynamical systems. Furthermore, it would be desirable to analyze the statistics of extremes generated from realistic physical models describing hydrodynamic or chemical chaos, or from models of atmospheric circulation. More importantly, the experimental data available on extreme values should be reconsidered in the light of the results reported in this work: in particular, the possibility of using extreme value distributions as a tool to obtain qualitative and quantitative measures that differentiate between deterministic chaos and random processes should be assessed. This is likely to provide new insights into the challenging problem of the prediction of extreme events.

ACKNOWLEDGMENTS

We are indebted to M. Malek Mansour, M. Mareschal, J. W. Turner, and C. Van den Broeck for helpful discussions. This work is supported, in part, by the SSTC of Belgium under the Global Change and Pôles d'Attraction Interuniversitaires programs and by the European Commission under the Environment and the Human Capital and Mobility programs.

REFERENCES

1. K. Lindenberg and B. J. West, *J. Stat. Phys.* **42**:201 (1986).
2. T. A. Buishand, *Stat. Neerland.* **43**:1 (1989).

3. E. J. Gumbel, *Statistics of Extremes* (Columbia University Press, New York, 1958).
4. J. Galambos, *The Asymptotic Theory of Extreme Order Statistics* (Wiley, New York, 1978).
5. M. R. Leadbetter and H. Rootzén, *Ann. Prob.* **16**:431 (1988).
6. M. R. Leadbetter, G. Lindgren, and H. Rootzén, *Extremes and Related Properties of Random Sequences and Processes* (Springer-Verlag, New York, 1983).
7. G. Nicolis and I. Prigogine, *Exploring Complexity* (Freeman, San Francisco, 1989).
8. C. Nicolis and G. Nicolis, eds., *Irreversible Phenomena and Dynamical Systems Analysis in the Geosciences* (Reidel, Dordrecht, 1987).
9. E. N. Lorenz, *Tellus* **36A**:98 (1984).
10. P. Bergé, Y. Pomeau, and C. Vidal, *L'ordre dans le chaos* (Hermann, Paris, 1984).
11. H. G. Schuster, *Deterministic Chaos*, 2nd ed. (VCH Verlag, Weinheim, 1988).
12. C. Gyorgyi and P. Szepfalusy, *Z. Phys. B. Cond. Matter* **55**:179 (1984).
13. P. C. Hemmer, *J. Phys. A: Math. Gen.* **17**:L247 (1984).
14. N. G. de Bruijn, *Asymptotic Methods in Analysis* (Dover, New York, 1981).